Recycling lithium mine tailings in the production of low temperature (700-900 ºC) ceramics: effect of ladle slag and sodium compounds on the processing and final properties

Patrick N. Lemougna*[1], Juho Yliniemi [1], Arnold Ismailov[2], Erkki Levanen[2], Pekka Tanskanen[3], Paivo Kinnunen[1], Juha Roning [4] and Mirja Illikainen[1]

[1]Faculty of Technology, Fiber and Particle Engineering Unit, PO Box 4300, 90014 University of Oulu, Finland.
[2]Materials Science, Faculty of Engineering and Natural Sciences, Tampere University,
P.O. Box 599, FI-33101 Tampere, Finland.
[3]Process Metallurgy Research Unit, University of Oulu, P.O. Box 4300, 90014 Oulu, Finland.
[4]InfoTech Oulu, Faculty of Information Technology and Electrical Engineering, Biomimetics and Intelligent Systems Group (BISG), University of Oulu, Oulu, Finland

*Corresponding author: Patrick.LemougnaNinla@oulu.fi

Abstract:

This paper deals with the valorization of quartz and felspar rich lithium mine tailings (QFS) in the development of construction materials. Ladle slag was used as green strength increasing agent. Sodium hydroxide and carbonate were used as fluxing agents to allow sintering at 700 - 900 ºC. Of these, sodium hydroxide was found to be the more efficient. The sintered ceramics were characterized by X-ray diffraction, scanning electron microscopy, compressive test, water absorption, apparent density and dilatometry; the results were found to comply with ASTM C62-99 specifications for building brick, and interesting for a sustainable use of resources.

Key words: Lithium mine tailings; ladle slag; ceramic; fluxing agent; sodium compounds; building applications

1. Introduction

The management of industrial by-products remains a challenging issue and the search for their recycling has become a recommended practice aiming to reduce the disposal cost and protect the environment [1–4]. Among these industrial by-products, mine wastes are currently one of the most generated in the world. Globally, they are estimated at 20-25 billion tons per year, of which 5 to 7 billion tons are mine tailings [2,3], the rest being mainly waste rocks. Mine tailings contain the non-valuable minerals rejected during the ore beneficiation process. Considering resources depletion and environment preservation, increasing pressures are supporting the need for recycling mine tailings. Among the utilization options, construction materials were found to be able to absorb a large quantity of suitable industrial by-products [5–7], with additional benefit in mitigating depletion of natural resources used as feedstock for building industry.

Accordingly, many studies were carried out on the valorization of mine tailings for the production of building materials, using several methods including ceramic processing [8–13]. For instance, Taha et al. [13] investigated the use of coal mine tailings in fired bricks production and observed a very interesting ornamental looks and acceptable mechanical properties for bricks fired at 1020 ºC with no other raw materials. Ahmari and Zhang [8] studied the feasibility of utilizing copper mine tailings for the production of eco-friendly bricks based on geopolymer technology. The procedure they used included mixing the tailings with an alkaline sodium hydroxide solution (10 - 15 M), forming the brick by compressing the mixture within a mold and curing the brick at 60–120 °C. Their results showed that copper mine tailings can be used to produce eco-friendly bricks meeting ASTM requirements. Chen et al. [14] studied the production of fired bricks from hematite mine tailings, by mixing it with fly ash and clay and obtained good quality fired bricks at 980–1050 ºC, with mechanical strength and water absorption of 20–23 MPa and 16–18%, respectively, and other physical properties meeting the Chinese Fired Common Bricks Standard (GB/T5101-2003).

Little information is available on the valorization of lithium mine tailings. Lithium is an essential metal with widespread applications including rechargeable lithium ion batteries for energy storage, electric mobility and cordless devices, glasses, ceramics, greases and rubbers [15–17]. Lithium demand is increasing, and its global production estimated at about 175 000 LCE tons (Lithium Carbonate Equivalent tons) in 2015 is expected to reach 650 000 tons in 2025 and 1 Mt in 2029 [16,18]. Spodumene ($LiAl(SiO_3)_2$,), with the stoichiometric chemical composition of 8.0 wt% Li_2O, 27.4 wt% Al_2O_3 and 64.6 wt% SiO_2 is the major source of hard rock based commercial lithium. It is usually found in nature in pegmatite deposits associated with quartz, feldspars and micas [20,21]. Due to the increasing global demand of lithium, quartz and feldspar rich tailings i.e. quartz-feldspar sand (QFS) from lithium ore processing is likely to be more generated in near future. For instance, Keliber Oy company is projecting to generate about 350 000 tons/ year of quartz and feldspar rich tailings (QFS) in the near future [22]. The reuse of such tailings also agrees with the concept of circular economy, aiming to capitalize material flow recycling while considering economic growth and sustainable development [23–25].

The present paper deals with the valorization of lithium mine tailings (quartz feldspar sand; QFS) in the production of low temperature ceramics for potential building applications. The ceramic processing option was chosen due to the presence of albite and microcline in the QFS.

Ladle slag (LDS), an under-utilized crystalline metallurgical residue [26–28], was tested as green strength increasing agent. Sodium carbonate and sodium hydroxide were used as fluxing agents to produce low temperature ceramics at 700-900 °C. In traditional ceramics, the vitrification that generally starts from 900 °C is marked by the melting of some solid phases that binds the remaining solid particles and increases the bonding strength [29–31]. The use of fluxing agents helps to enhance sintering or decrease the vitrification temperature [32,33].

The QFS and LDS were characterized by XRD and TG/DSC analysis and the synthetized materials were characterized by X-Ray diffraction, Scanning electron microscopy and Dilatometry analysis.

The suitability of the synthetized materials for building applications was assessed by the determination of their compressive and flexural strength, apparent density and water absorption.

2. Experimental

2.1. Materials

The chemical composition of QFS and LDS used in this study is presented in Table 1.

The oxide composition was determined by X-ray fluorescence, using a wavelength dispersive XRF spectrometer (AxiosmAX, PANanalyctical). The QFS, the final tailings from spodumene flotation, was received from Keliber Oy, Finland and was found to be environmentally-friendly according to Finnish regulation, with no hazardous elements, as shown by the results on the leaching test presented in Table 2. The LDS was also provided by a Finnish company. The particle size information of QFS and LDS, analysed by a laser diffraction technique using a Beckman Coulter 13 LS 320 particle size analyser is presented in Table 3.

The particle size of QFS used was significantly reduced after grinding, from d_{50} of 171.4 µm to d_{50} of 10.70 µm. This final particle size was close to the one of LDS, which presented a d_{50} of 12.34 µm. Sodium carbonate (99% Na_2CO_3) and sodium hydroxide (99% NaOH) of laboratory grade were used.

2.2. Specimens preparation

The preparation of the fresh mixtures was performed by mixing QFS, LDS, sodium hydroxide or sodium carbonate and water. The details on the mix proportioning are presented in Table 4.

The compositions containing both QFS and LDS were first dry mixed. Sodium compound was dissolved in water and the alkaline solution was mixed with the dry powder for 5 min, using an electric mixer at 3000 rpm, until obtaining a homogenous paste. Samples containing 0 wt% sodium compound were prepared by mixing QFS and QFS/LDS with an appropriate amount of water

(Table 4). The samples were then cast in rectangular alloy molds (80×20×20 mm). The alloy molds were vibrated on a vibration table for 1 min to remove air bubbles and left for 24h at room temperature (~20 ºC), then 24 hours at 105 ºC, before being sintered at 700, 800 and 900 ºC; heating rate of 2 ºC/min with a dwell time of 2 hours at each temperature. The heating rate of 2 ºC/min was adopted to reduce the sensitivity to form cracks, due to rapid residual water loss or rapid solid-state reaction during heating. The heating temperature range of 700-900 °C was explored to check if the fluxing agents can lower the sintering temperature below the one of traditional ceramics which are usually sintered around 900-1050 ºC [10,31,34]. This temperature range was also adopted based on the results obtained from preliminary investigations.

2.3. Characterization methods

2.3.1. Compressive and flexural strength, water absorption and apparent density

The three-point flexural test of specimens was performed using a Zwick testing machine with a maximum load of 100 kN and a loading rate of 0.05 kN/s; sample dimensions: length 80 mm, width 20 mm, and height 20 mm. For each composition, three replicates specimens were tested. The supports span was 40 mm. The flexural strength (δ) was determined using the equation below:

$$\delta = 3FL/2bd^2$$

Where: δ is flexural strength in N/mm^2; F is maximum load in N; L is supports distance in mm; b is width of the tested beam in mm and d is height of the tested beam in mm.

The compressive strength was done using the same device, with a loading rate of 2.4 kN/s, height of the sample 20 mm and compressed surface 20 × 20 mm^2. For each composition, three replicates specimens were tested, and the average was regarded as the representative value. The error bar indicates the standard deviation between specimens.

Water absorption was determined after samples immersion in deionized water for 24 hours and apparent density, using the Archimedes' principle according to SFS-EN 1936 standard.

2.3.2. XRD analysis

The samples were powdered and examined by X-ray diffraction using a Rigaku Smartlab diffractometer, with a Cu K-beta radiation, step width of 0.02º, scan speed 2.0156 º/min, 2θ range of 5–80º, operated at 200 mA and 45 kV. The quantification of the crystalline phases was performed by the Rietveld refinement method using 10 wt% rutile (TiO_2) as internal standard.

2.3.3. SEM/EDX analysis

Polished sections were made from QFS and synthetized specimens. Scanning Electron Microscopy (SEM) and Energy Dispersive X-ray Spectroscopy (EDX) (Zeiss Ultra Plus) were used to study the microstructure of the materials and to analyze chemical composition of the phases. Analyses were performed with a backscatter electron detector with 15 kV acceleration voltage and the working distance was about 8.5 mm. The sample surfaces were coated with carbon prior to measurements.

2.3.4. TG/DSC and dilatometry analysis

TG/DSC analysis was performed with a simultaneous TG/DSC measurement in air, using a NETZSCH STA 449F3 TG/DSC instrument at a constant heating rate of 5 °C/min. The samples were heated from room temperature to 1600 °C.

Dilatometry analysis was carried out on selected samples that presented acceptable mechanical properties. The samples were molded and cut to 8×8×10 mm and the experiment was performed on a NETZSCH DIL 402 Expedis dilatometer. Prepared samples were heated in two cycles: Firstly to 800 ºC at 2 ºC/ per min, 2 hours dwell time, and secondly at 900 ºC, heating rate 2 ºC/ per min and 2 hours dwell time. The heating chamber was open ended, but a constant flow of nitrogen (40 ml/min) was used as the purge gas to prevent unwanted gaseous/evaporated matter getting into the measurement chamber, which was separated from the heating chamber where the sample was put.

3. Results and discussion

3.1. Compressive and flexural strength, water absorption and apparent density

The compressive strength of selected green specimens (not heated but dried in the oven at 105 ºC for 24 hours) is presented in Figure 1.

All the samples were found to set after 24 hours at room temperature, albeit samples made of QFS without LDS addition were weaker and required to be gently handled during unmolding operation. After drying at 100 ºC, the positive effect of LDS addition on the green strength was observed by an increase in the compressive strength to about 3 MPa compared to 0 MPa for the specimens made of 100 wt% of QFS. The strength of the specimens containing LDS was further increased with the addition of sodium hydroxide while formulations made with 100 wt% of QFS and sodium hydroxide presented compressive strength below 1 MPa. The positive effect of LDS on the green strength is interesting and useful for specimens handling before sintering. These results are in agreement with previously reported studies on LDS which was found to be able to produce materials with good mechanical properties by alkali activation [26,27]. However, the percentage used in this study was too low to allow a good stability of the materials.

The compressive strength of the sintered specimens is presented in Figure 2 (2a and 2b for specimens containing LDS, 2c and 2d for specimens made of QFS only).

Compressive strength of the materials is observed to significantly vary according to specimen's composition from about 0.3 MPa to about 55 MPa.

The main reasons for strength variation were the type and amount of the sodium compounds as well as the sintering temperature. All the samples prepared with sodium hydroxide performed well in comparison to their counterparts prepared with sodium carbonate, although the Na_2O/Al_2O_3 molar ratio was almost the same in both type of formulations. Strength was also found to increase with the increase in the amount of sodium compound mainly in the specimen prepared with sodium

hydroxide. For specimens prepared with sodium carbonate, no significant increase in strength was observed for formulations prepared with more than 3 wt% of sodium carbonate.

The temperature for highest strength development was 900 ºC in specimens prepared with low amounts of sodium compounds. However, strength did not significantly increase or showed a slight reduction between 800 ºC and 900 ºC for formulations prepared with more than 3 wt% of sodium carbonate and 5 parts (~5 wt%) of sodium hydroxide. The composition nº 9, prepared with 7 parts (~7 wt%) of sodium hydroxide presented the highest compressive strength, with the values of about 52, 55 and 46 MPa at 700, 800 and 900 ºC respectively. This formulation also presented a slight deformation at 900 ºC. The compressive strength of the specimens containing 10 wt% LDS and 1 part (~1 wt%) of sodium compounds were all below 10 MPa at 700 - 900 ºC (Figure 2a and 2b). Sample nº 1, made of 90 wt% QFS and 10 wt% LDS with no sodium compound presented a compressive strength of about 2, 3 and 8 MPa at 700, 800 and 900 ºC respectively. This highlights the positive effect of sodium addition in the sintering of the specimens and strength development.

The compressive strengths of specimens prepared with QFS and sodium compounds without addition of LDS are presented in Figures 2c and 2d. All the samples prepared with QFS and sodium carbonate presented a compressive strength below 10 MPa. However, the compressive strength of specimens containing 1 and 3 parts NaOH were superior to their counterpart containing LDS, suggesting that LDS addition was mainly beneficial only as green strength increasing agent. Actually, industrial byproducts or natural raw materials used for fired bricks usually content about 50-70% SiO_2 [8,13,35–38]. The presence of alkaline and alkaline earth in these materials is beneficial for sintering, favouring at lower temperature the formation of intergranular liquid phase, which allows mass transport phenomena and local binding of the solid grains [37]. Hence, LDS addition is likely not to have positively affected the sintering reactions. This is suggested to be linked to its superior refractory character, in comparison to QFS as show in the DSC analysis in the

next section. The compressive strength of building materials such as bricks is one of the most important engineering properties. The minimum requirement of compressive strength for building bricks varies depending on standards and the working conditions that will be applied to the bricks [31,39,40]. For instance, IS 1077: 1992 specifies the minimum compressive strength of common burnt clay building bricks from 3.5 to 35 MPa, depending on brick grade or targeted application [40] . Meanwhile, ASTM C62-99 specifies the minimum of 10.3 MPa for bricks subjected to negligible weathering conditions and 20.7 MPa for bricks subjected to severe weathering conditions [39].

From Figure 2, it is also noted that the compressive strength values of many compositions were above 20 MPa, satisfying the minimum requirement of compressive strength for many building materials, including paving bricks subjected to light traffic [6,37,39,41].

Based on the compressive strength results, some compositions were considered for flexural strength and further characterization.

Figure 3 presents the flexural strength of compositions prepared with 3, 5 and 7 parts wt% of sodium compounds at 800 and 900 ºC: composition 4 (90 QFS, 10 LDS, 3 parts Na_2CO_3); 5 (90 QFS, 10 LDS, 3 parts NaOH); 6 (90 QFS, 10 LDS, 5 parts Na_2CO_3); 7 (90 QFS, 10 LDS, 5 parts NaOH); 8 (90 QFS, 10 LDS, 7 parts Na_2CO_3) and 9 (90 QFS, 10 LDS, 7 parts NaOH). Almost similarly to the compressive strength trend, the flexural strength was found to increase with the increase of the sodium compound and sintering temperature, and higher flexural strength were obtained with specimens containing sodium hydroxide, with a maximum value of about 14 MPa at 900 ºC. It is also noted that the shapes of the failure curves are all typical of brittle materials like ceramics.

The apparent density and water absorption values of referred compositions are presented in Figure 4.

The water absorption values were in the range of 4 to 20%, decreasing with the increase of the sintering temperature and the amount of alkali content in the materials. The water absorption values of composition nº 9, containing about 7 wt% of sodium hydroxide varied from about 10% at 700 ºC to 4% at 900 ºC, while its counterpart made with sodium carbonate varied from about 19% at 700 ºC to 15% at 900 ºC. This confirms again a higher fluxing effect of sodium hydroxide in comparison to sodium carbonate. The higher performance of sodium hydroxide in comparison to sodium carbonate can be ascribed to the more aggressive character (higher alkalinity) of sodium hydroxide [42,43], which favored some dissolution of QFS and LDS during the mixing operation and led to better sintering reactions. Apparent density values were in the range of 1.65 to 2 $g.cm^{-3}$, increasing with the sintering temperature, at variance to water absorption. Lower densities and higher water absorption values were obtained with specimens prepared with sodium carbonate and the trend of increase of density with the increase of sintering temperature was less obvious in comparison to compositions prepared with sodium hydroxide. This may be linked to carbonate dissociation and release of CO_2 during sintering, which contributed in the increase of porosity and led to matrix with lower strength.

Water absorption is an important parameter for building materials such as bricks, since it influences properties such as permeability and durability [31]. However, that will still depend on the targeted application of the bricks. For instance, according to ASTM C62-99 specifications for building brick [39], there is no limit for water absorption for bricks that will be subjected to negligible weathering, while those to be subjected to severe weathering should present 17% as maximum value of water absorption. Hence, only formulations prepared with 3 -7 wt% NaOH that presented low water absorption and adequate strength could be used in severe weathering conditions.

3.2. Characterization of QFS and LDS

The XRD spectra of QFS and LDS are presented in Figure 5.

The QFS presented crystalline reflections mainly ascribed to quartz: SiO_2 (Pdf no 04-014-7568) and albite:_$Na_{0.98}Ca_{0.02}Al_{1.02}Si_{2.98}O_8$ (Pdf n° 04-017-1022). Microcline: $KAlSi_3O_8$ (Pdf no 04-007-8600) and traces of muscovite: $K_{0.8}Na_{0.2}Fe_{0.05}Al_{2.95}Si_{3.1}O_{10}(OH)_2$ (Pdf no 04-012-1906) were also observed. The LDS presented crystalline reflections ascribed to calcio-olivine: Ca_2SiO_4 (Pdf no 04-006-8894), mayenite_ $Ca_{12}Al_{14}O_{32.55}$ (Pdf no 04-015-5594), Periclase_ MgO (Pdf no 04-005-4664), Calcium Aluminum Oxide_Ca_3 Al_2 O_6 (Pdf no 04-007-4797) and Calcium Magnesium Aluminum Silicon Oxide_$Ca_{10}Mg_{1.5}Al_{13}Si_{1.5}O_{34}$ (Pdf no 04-009-3800). These results are in agreement with the origin of the QFS which is from spodumene ore, known to be commonly associated with minerals such as quartz and micas, as well as albite and microcline felspars [19,20].

The TG/DSC analysis of QFS and LDS is presented in Figure 6.

Both materials showed a relatively good thermal stability, with a mass loss of about 1.1 and 0.5% at 1600 °C for QFS and LDS respectively. The DSC curve of QFS presented an endothermic peak around 573 ºC ascribed to α - β quartz phase transformation [44]. A broad endothermic peak is observed around 1200 ºC likely due to the initial eutectic melting of the sample as almost no mass loss is concomitantly observed. The broadness of the peak is an indication of multicomponent phases in QFS. For the case of LDS, the peak ascribed to the melting of the sample was observed around 1300 ºC, indicating a higher refractory behavior. This agrees with the chemical composition of LDS which contains fewer amounts of alkali elements.

3.3. Phase composition of the synthetized materials

Heating QFS to 900 ºC has mainly led to the disappearance of the initial traces of muscovite transformed to amorphous structure with the loss of (OH) groups, and the formation of traces of anorthoclase_$K_{0.224}$ $Na_{0.710}$ $Ca_{0.069}$ $Al_{1.036}$ $Si_{2.952}$ O_8 (pdf no 04-013-2165), nepheline_ $K_{0.7}$ $Na_{2.75}$ $Ca_{0.15}$ $Al_{3.75}$ $Si_{4.25}$ O_{16} (pdf no 04-011-2330) and amorphous phases (Figure 7).

Anorthoclase is an intermediate member of the high albite – sanidine alkali feldspar solid solution series while nepheline is a feldspathoid mineral characteristic of alkaline rocks [45,46]. However, albite, microcline and quartz reflections were maintained in the samples, but their crystalline reflections were found to reduce with the increase of sodium content, because of the formation of advanced melting in the samples, generating an amorphous phase. It is also noted that specimens containing 10 wt% LDS presented almost the same crystalline reflections as specimens made of 100 wt% QFS. This was due to the lower crystalline reflections of LDS in comparison to QFS, as shown in Figure 5.

The estimated percentage of crystalline phases using the Rietveld refinement method is presented in Figure 8, showing an increase in the amorphous content with the increase of sodium in the specimen, in agreement with the reduction of crystalline reflections in Figure 7. For instance, quartz proportion was found to reduce from about 30% in QFS to about 10% in composition 9 (~7 wt% NaOH) treated at 900 ºC (Figure 8).

Formation of feldspathoids and quartz /silica reduction in matrixes containing aluminosilicates and Na_2O during ceramic processing has been previously reported [37,47]. In a study at 1000 ºC of Na_2O–SiO_2–Al_2O_3 system related to reactions of sodium containing minerals in ash melting process, Wang et al., [47] noticed that with rising content of Na_2O, the fusion temperature of the ash was reduced, and albite was generated gradually from about 900 ºC, then transformed to nepheline after SiO_2 was consumed following equations 1 and 2 :

$$Na_2O + Al_2O_3 + 6SiO_2 \longrightarrow 2NaAlSi_3O_8 \text{ (Albite)} \quad (1)$$

$$NaAlSi_3O_8 \text{ (Albite)} + Al_2O_3 + Na_2O \longrightarrow 3NaAlSiO_4 \text{ (Nepheline)} \quad (2)$$

In view of the reduction of crystalline reflection of quartz in the composition with higher content of sodium compound at 900 ºC, onset of similar reactions is likely to have occurred in the specimen. However, the limited amount of nepheline found in the specimens (about 4 %) is most likely from local reactions. Hence, partial melting of some phases due to eutectic formations, increasing interfacial bonding between material particles is most likely to has been responsible of strength development. This is supported by the increasing amount of the amorphous phase with the increase of sodium content in the system and is further evidenced in the microstructural characterization presented in the next section.

3.4. Microstructural characterization

The back scattered scanning electron image of the powdered QFS used is presented in Figure 9.

The QFS analyzed in the XRD section was found to contain quartz, albite, microcline and a few amount of muscovite. From the chemical formula of these minerals, weight percentage of each element can be assessed. Quartz contains about 46.74 wt% of Si and 53.26 wt% of O. Albite contains about 8.30 wt% Na, 0.76 wt% Ca, 10.77 wt% Al, 31.50 wt% of Si and 48.66 wt% of O. Microcline contains about 14.05 wt% of K, 9.69 wt% of Al, 30.27 wt% of Si and 45.99 wt% of O. Point analysis of some particles in the QFS image (Figure 9) is summarized in Table 5.

The comparison of the information from Table 4 and the XRD analysis allowed to ascribe and identify quartz, albite and microcline in the powder. Muscovite was not identified, possibly due to its lowest amount (~ 4.7%) in QFS.

The back scattered images of compositions 3, 9 and 14 treated at 900 ºC are presented in Figure 10.

A clear difference was observed between the images of each composition. On the image of composition 3 (prepared with 1 part NaOH) which presented a very low compressive strength, relics of QFS and LDS particles are bigger and their boundaries are well marked. Furthermore, the size of the relic of QFS particles is very close to the one of powdered QFS, because of low sintering reactions between particles. Almost any evidence of material melting can be observed.

The image of compositions 9 and 14, containing 7 and 3 parts of NaOH respectively, showed smaller roundish shaped boundaries relics of QFS particles and good interfacial bonding between these relics and the amorphous matrix between the particles. This is a results of a better sintering reaction which was favored by the increase of sodium content in these compositions. Higher magnification images of compositions 3 and 9 are presented in Figure 11, with complementary information from the Figure presented in Table 6.

The compositions 3 and 9 were all prepared with QFS (90 wt%) and LDS (10 wt%). The only difference between these compositions is the proportion of sodium (7 parts in composition 9 and 1 part in composition 3). The contrast in these two images is then only linked to the difference in sodium proportion between the two compositions. A more compact and good interfacial bonding between relic of starting particles is very well highlighted in the image of composition 9. A 10µm line analysis (A-B) from a relic of quartz particle to the amorphous phase showed that the reduction of silica in the line is gradual at the interfacial zone, while the increase in the content of K, Ca, Al and Na elements is also gradual, further supporting a very good interfacial bonding, which has favored a good compressive and flexural strength. The elemental weight composition of selected points in Figure 11 is presented in Table 6.

Point analysis of composition 9 showed that the composition of the glassy phase melted (points 3 to 8) around the relic of particles is almost constant. This agrees with the hypothesis of partial melting

suggested in the XRD section. The thermal agitation has favored atoms migration in the melted phase which presented a close atomic proportion of Al, Si, Na, K and Ca in the points selected. The potassium content in the melted phase was about 3 to 4 wt% and suggests a great participation of microcline and muscovite in the melting. This was also confirmed by XRD analysis.

The amount of the glassy phase was lower for composition 14, due to the lower amount of Na in comparison to composition 9. Indeed, in aluminosilicate glasses, SiO_2 is a network former while Al_2O_3 keeps the viscosity high above the glass transition temperature and can be network former or modifier. Na_2O is a network modifier and lower the glass transition temperature and the viscosity in the melt [48,49]. Points 16-18 are in a LDS particle of composition 3 (90 wt% QFS +10 wt% LDS + 1 part NaOH) after thermal treatment at 900 °C. The analysis of these points showed that LDS particles are made of several crystal phases, at variance to QFS where most of the particles were found to be made of a single crystalline phase.

3.5. Dilatometry analysis

The dilatometry curves of samples nº 7 (90 QFS, 10 LDS, 5 parts NaOH), 8 (90 QFS, 10 LDS, 7 parts Na_2CO_3), 9 (90 QFS, 10 LDS, 7 parts NaOH) and 14 (100 QFS, 3 parts NaOH) are presented in Figure 12.

The first circle represents the sintering shrinkage while the second cycle gives an indication on the materials stability until 900 ºC. On the heating curves, a sharp transient increase in expansion is observed around 573 ºC, due to α - β inversion of quartz, in agreement with the DSC results and reported studies on materials containing quartz [50]. For all the selected compositions, the materials only expand until about 600 ºC before starting to shrink. This suggests that no or minor sintering reactions occurred until 600 ºC, confirming the choice of 700°C reasonable as minimum sintering temperature that could allow some sintering reactions. The sintering shrinkages (DL/Lo) at 800 ºC

were about -0.5%, -0.7% and -0.8% for specimens nº 7 (~ 5 wt% of sodium hydroxide), nº8 (~ 7 wt% of sodium carbonate) and nº9 (~ 7 wt% of sodium hydroxide) respectively. Specimen nº 14 (~ 3 wt% of sodium hydroxide), presented the lowest DL/Lo of about -0.25%. The permanent shrinkage was also significant during the dwell time indicating ongoing of sintering reactions and was more marked for specimens prepared with sodium hydroxide, as a result of the better fluxing performance of NaOH in comparison to Na_2CO_3. The values of DL/Lo after 800 ºC treatment are comparable with reported values of shrinkage of fired brick materials based on industrial wastes [36]. During the second heating cycle, the sample expanded almost linearly up to about 800 ºC before resuming the sintering reactions started in the first cycle. Permanent shrinkage mostly occurred during the heating above 800 °C and dwell in 900 °C for samples containing LDS (Compositions no 7, 8, 9), while additional compacting during cooling was observed in sample 14 made of 100 wt% QFS (Figure 13). This suggests that sample 14 would undergo some significant additional shrinkage if dwell time was increased while other mixtures would have been less affected. The likely reason for that is the higher content in sodium/potassium in QFS, in comparison to LDS.

The coefficient of thermal expansions between 600 and 800 ºC were about $11.48\times10^{-6}\,C^{-1}$, $11.24\times10^{-6}\,C^{-1}$ $11.95\times10^{-6}\,C^{-1}$ and $9.18\times10^{-6}\,C^{-1}$ for composition nº 7, 8, 9, and 14 respectively. The thermal expansion coefficient of a glass decreases with the increase of the rigidity of the glass network and is linked to the amount of additives which affect the asymmetry of the amplitude of thermal vibrations [51]. This agrees and explains the lower coefficient of thermal expansion for sample containing lower sodium compound. Sodium hydroxide is also found to favor higher coefficient of thermal expansion, in comparison to sodium carbonate. The coefficients of thermal expansion obtained are in the same order of magnitude as some reported values for inorganic polymers and ceramics [51–53].

The thermal stability of the materials was globally improved after the first heating cycle and the values of DL/L_o in the second cycle were about -0.2%, -0.35%, -0.5% and -0.35% for specimens n° 7, 8, 9 and 14 respectively. The physical evolution of materials during heating is an important factor to be considered for building and refractory materials [41,54]. The thermal stability of the materials until 800- 900 ºC was better than those of some inorganic polymers (geopolymer) [48,53,54] and suggests a possible suitability of the materials for low temperature refractory applications, until about 800 ºC.

The results presented above clearly demonstrate that QFS can be used in the production of low temperature building ceramics, with some advantages for sustainability. All felsic mining i.e. tailings rich in quartz and felspars may also be suitable to be valorised using the same approach. These tailings include molybdenum ore tailings, gold ore tailings and quartz ore tailings [55].

4. Conclusion

The management of mining wastes remains an important issue to be addressed. Low temperature (700-900 ºC) ceramics with interesting physical properties were successfully prepared from quartz, feldspar sand lithium mine tailings (QFS). Ladle slag (LDS) was used as increasing green strength agent in some compositions. Sodium carbonate and sodium hydroxide were used as fluxing agent, in the proportion range of 1 to 7 per 100 parts of the dry mass of QFS/LDS. Sodium hydroxide was found to perform better as fluxing agent, leading to specimens with higher compressive strength, higher density and lower water absorption. The maximum values of compressive and flexural strength were 55 and 14 MPa respectively, while water absorption and apparent density values ranged from about 4 to 19% and 1.65 to 2 $g.cm^{-3}$ respectively. Most of the compositions prepared with 3 - 7 wt% NaOH presented good properties, meeting the requirement of building brick according to ASTM C62-99. Scanning electron micrograph of the sintered ceramics presented a

dense microstructure with some relic of starting materials. Densification resulted from solid state reactions and partial melting of phases, with the reduction of crystallinity and quartz proportion in the matrix. Dilatometry analysis showed that the relative length change (DL/L_o) of the specimens was between -0.6% and -1.5% after two sequential heating cycles, the first at 800 and the second at 900 ºC, with coefficient of thermal expansions of 9 to 12×10^{-6} C^{-1} between 600 and 800 ºC and higher sintering shrinkage for specimens prepared with NaOH.

The overall results are of great interest for sustainability and the valorization of QFS and similar tailings in the production of low temperature ceramics for building applications.

Acknowledgements

This work was performed under the framework of the "GEOBOT" project, supported by the European Regional Development Fund (ERDF), Pohjois-Pohjanmaa Council of Oulu Region and Vipuvoimaa EU:lta 2014-2020 and companies Boliden Harjavalta Oy, Keliber Oy and Saint-Gobain Finland Oy.

References

[1] D. Dodoo-Arhin, R.A. Nuamah, B. Agyei-Tuffour, D.O. Obada, A. Yaya, Awaso bauxite red mud-cement based composites: Characterisation for pavement applications, Case Studies in Construction Materials. 7 (2017) 45–55. doi:10.1016/j.cscm.2017.05.003.

[2] P. Kinnunen, A. Ismailov, S. Solismaa, H. Sreenivasan, M.-L. Räisänen, E. Levänen, M. Illikainen, Recycling mine tailings in chemically bonded ceramics – A review, Journal of Cleaner Production. 174 (2018) 634–649. doi:10.1016/j.jclepro.2017.10.280.

[3] J. Kiventerä, L. Golek, J. Yliniemi, V. Ferreira, J. Deja, M. Illikainen, Utilization of sulphidic tailings from gold mine as a raw material in geopolymerization, International Journal of Mineral Processing. 149 (2016) 104–110. doi:10.1016/j.minpro.2016.02.012.

[4] M. Saeli, D.M. Tobaldi, M.P. Seabra, J.A. Labrincha, Mix design and mechanical performance of geopolymeric binders and mortars using biomass fly ash and alkaline effluent from paper-pulp industry, Journal of Cleaner Production. 208 (2019) 1188–1197. doi:10.1016/j.jclepro.2018.10.213.
[5] C. Klauber, M. Gräfe, G. Power, Bauxite residue issues: II. options for residue utilization, Hydrometallurgy. 108 (2011) 11–32. doi:10.1016/j.hydromet.2011.02.007.
[6] A.L. Murmu, A. Patel, Towards sustainable bricks production: An overview, Construction and Building Materials. 165 (2018) 112–125. doi:10.1016/j.conbuildmat.2018.01.038.
[7] T. Hertel, B. Blanpain, Y. Pontikes, A Proposal for a 100 % Use of Bauxite Residue Towards Inorganic Polymer Mortar, Journal of Sustainable Metallurgy. 2 (2016) 394–404. doi:10.1007/s40831-016-0080-6.
[8] S. Ahmari, L. Zhang, Production of eco-friendly bricks from copper mine tailings through geopolymerization, Construction and Building Materials. 29 (2012) 323–331. doi:10.1016/j.conbuildmat.2011.10.048.
[9] A. Al-Fakih, B.S. Mohammed, M.S. Liew, E. Nikbakht, Incorporation of waste materials in the manufacture of masonry bricks: An update review, Journal of Building Engineering. 21 (2019) 37–54. doi:10.1016/j.jobe.2018.09.023.
[10] N.V. Boltakova, G.R. Faseeva, R.R. Kabirov, R.M. Nafikov, Yu.A. Zakharov, Utilization of inorganic industrial wastes in producing construction ceramics. Review of Russian experience for the years 2000–2015, Waste Management. 60 (2017) 230–246. doi:10.1016/j.wasman.2016.11.008.
[11] M.W. Gitari, S.A. Akinyemi, R. Thobakgale, P.C. Ngoejana, L. Ramugondo, M. Matidza, S.E. Mhlongo, F.A. Dacosta, N. Nemapate, Physicochemical and mineralogical characterization of Musina mine copper and New Union gold mine tailings: Implications for fabrication of beneficial geopolymeric construction materials, Journal of African Earth Sciences. 137 (2018) 218–228. doi:10.1016/j.jafrearsci.2017.10.016.
[12] S. Solismaa, A. Ismailov, M. Karhu, H. Sreenivasan, M. Lehtonen, P. Kinnunen, M. Illikainen, M.L. Räisänen, Valorization of Finnish mining tailings for use in the ceramics industry, Bulletin of the Geological Society of Finland. Vol. 90, (2018) 33-54.
[13] Y. Taha, M. Benzaazoua, R. Hakkou, M. Mansori, Coal mine wastes recycling for coal recovery and eco-friendly bricks production, Minerals Engineering. 107 (2017) 123–138. doi:10.1016/j.mineng.2016.09.001.
[14] Y. Chen, Y. Zhang, T. Chen, Y. Zhao, S. Bao, Preparation of eco-friendly construction bricks from hematite tailings, Construction and Building Materials. 25 (2011) 2107–2111. doi:10.1016/j.conbuildmat.2010.11.025.
[15] H. Hao, Z. Liu, F. Zhao, Y. Geng, J. Sarkis, Material flow analysis of lithium in China, Resources Policy. 51 (2017) 100–106. doi:10.1016/j.resourpol.2016.12.005.
[16] G. Martin, L. Rentsch, M. Höck, M. Bertau, Lithium market research – global supply, future demand and price development, Energy Storage Materials. 6 (2017) 171–179. doi:10.1016/j.ensm.2016.11.004.
[17] P. Meshram, B.D. Pandey, T.R. Mankhand, Extraction of lithium from primary and secondary sources by pre-treatment, leaching and separation: A comprehensive review, Hydrometallurgy. 150 (2014) 192–208. doi:10.1016/j.hydromet.2014.10.012.
[18] Swiss Resource Capital AG, Lithium Report 2017, (2017).
[19] G. Kuang, Y. Liu, H. Li, S. Xing, F. Li, H. Guo, Extraction of lithium from β-spodumene using sodium sulfate solution, Hydrometallurgy. 177 (2018) 49–56. doi:10.1016/j.hydromet.2018.02.015.
[20] M.G. Aylmore, K. Merigot, W.D.A. Rickard, N.J. Evans, B.J. McDonald, E. Catovic, P. Spitalny, Assessment of a spodumene ore by advanced analytical and mass spectrometry

techniques to determine its amenability to processing for the extraction of lithium, Minerals Engineering. 119 (2018) 137–148. doi:10.1016/j.mineng.2018.01.010.
[21] Y. Wang, G. Zhu, L. Zhang, D. Lu, L. Wang, Y. Zhao, H. Zheng, Surface dissolution of spodumene and its role in the flotation concentration of a spodumene ore, Minerals Engineering. 125 (2018) 120–125. doi:10.1016/j.mineng.2018.06.002.
[22] Keliber, Keliber Oy LITHIUM PROJECT Definitive Feasibility Study – Executive Summary, June 14, 2018, (2018).
[23] K. Winans, A. Kendall, H. Deng, The history and current applications of the circular economy concept, Renewable and Sustainable Energy Reviews. 68 (2017) 825–833. doi:10.1016/j.rser.2016.09.123.
[24] C. Sassanelli, P. Rosa, R. Rocca, S. Terzi, Circular Economy performance assessment methods: a systematic literature review, Journal of Cleaner Production. (2019). doi:10.1016/j.jclepro.2019.05.019.
[25] N.M. Gusmerotti, F. Testa, F. Corsini, G. Pretner, F. Iraldo, Drivers and approaches to the circular economy in manufacturing firms, Journal of Cleaner Production. (2019). doi:10.1016/j.jclepro.2019.05.044.
[26] E. Adesanya, K. Ohenoja, P. Kinnunen, M. Illikainen, Alkali Activation of Ladle Slag from Steel-Making Process, Journal of Sustainable Metallurgy. 3 (2017) 300–310.
[27] H. Nguyen, V. Carvelli, E. Adesanya, P. Kinnunen, M. Illikainen, High performance cementitious composite from alkali-activated ladle slag reinforced with polypropylene fibers, Cement and Concrete Composites. 90 (2018) 150–160. doi:10.1016/j.cemconcomp.2018.03.024.
[28] H. Nguyen, P. Kinnunen, V. Carvelli, M. Mastali, M. Illikainen, Strain hardening polypropylene fiber reinforced composite from hydrated ladle slag and gypsum, Composites Part B: Engineering. (2018). doi:10.1016/j.compositesb.2018.09.056.
[29] Z. Zhang, Y.C. Wong, A. Arulrajah, S. Horpibulsuk, A review of studies on bricks using alternative materials and approaches, Construction and Building Materials. 188 (2018) 1101–1118. doi:10.1016/j.conbuildmat.2018.08.152.
[30] V.G. Karayannis, Development of extruded and fired bricks with steel industry byproduct towards circular economy, Journal of Building Engineering. 7 (2016) 382–387. doi:10.1016/j.jobe.2016.08.003.
[31] V.V. Kulkarni, A.K. Golder, P.K. Ghosh, Production of composite clay bricks: A value-added solution to hazardous sludge through effective heavy metal fixation, Construction and Building Materials. 201 (2019) 391–400. doi:10.1016/j.conbuildmat.2018.12.187.
[32] R. Sokolář, L. Keršnerová, M. Šveda, The effect of different fluxing agents on the sintering of dry pressed porcelain bodies, Journal of Asian Ceramic Societies. 5 (2017) 290–294. doi:10.1016/j.jascer.2017.06.001.
[33] N. Chandra, N. Agnihotri, S.K. Bhasin, Sintering characteristics of talc in the presence of phosphatic and alkali carbonate sintering activators, Ceramics International. 30 (2004) 643–652. doi:10.1016/j.ceramint.2003.08.007.
[34] N. Dalkılıç, A. Nabikoğlu, Traditional manufacturing of clay brick used in the historical buildings of Diyarbakir (Turkey), Frontiers of Architectural Research. 6 (2017) 346–359. doi:10.1016/j.foar.2017.06.003.
[35] A. De Bonis, G. Cultrone, C. Grifa, A. Langella, V. Morra, Clays from the Bay of Naples (Italy): New insight on ancient and traditional ceramics, Journal of the European Ceramic Society. 34 (2014) 3229–3244. doi:10.1016/j.jeurceramsoc.2014.04.014.
[36] D. Eliche-Quesada, J.A. Sandalio-Pérez, S. Martínez-Martínez, L. Pérez-Villarejo, P.J. Sánchez-Soto, Investigation of use of coal fly ash in eco-friendly construction materials: fired clay bricks and silica-calcareous non fired bricks, Ceramics International. 44 (2018) 4400–4412. doi:10.1016/j.ceramint.2017.12.039.

[37] R. Taurino, A. Karamanov, R. Rosa, E. Karamanova, L. Barbieri, S. Atanasova-Vladimirova, G. Avdeev, C. Leonelli, New ceramic materials from MSWI bottom ash obtained by an innovative microwave-assisted sintering process, Journal of the European Ceramic Society. 37 (2017) 323–331. doi:10.1016/j.jeurceramsoc.2016.08.011.
[38] A. Viani, G. Cultrone, K. Sotiriadis, R. Ševčík, P. Šašek, The use of mineralogical indicators for the assessment of firing temperature in fired-clay bodies, Applied Clay Science. 163 (2018) 108–118. doi:10.1016/j.clay.2018.07.020.
[39] ASTM, ASTM C62-99: Standard Specification for Building Brick (Solid Masonry Units Made From Clay or Shale), (1999).
[40] Bureau of Indian Standards, New Delhi, IS:1077, Common Burnt Clay Building Bricks – Specification, (1992).
[41] P.N. Lemougna, K.J.D. MacKenzie, U.F.C. Melo, Synthesis and thermal properties of inorganic polymers (geopolymers) for structural and refractory applications from volcanic ash, Ceramics International. 37 (2011) 3011–3018. doi:10.1016/j.ceramint.2011.05.002.
[42] J.L. Provis, 4 - Activating solution chemistry for geopolymers, in: J.L. Provis, J.S.J. van Deventer (Eds.), Geopolymers, Woodhead Publishing, 2009: pp. 50–71. doi:10.1533/9781845696382.1.50.
[43] I. G, B. Singh, S. Deshwal, S.K. Bhattacharyya, Effect of sodium carbonate/sodium silicate activator on the rheology, geopolymerization and strength of fly ash/slag geopolymer pastes, Cement and Concrete Composites. (2018). doi:10.1016/j.cemconcomp.2018.12.007.
[44] D.S. Klimesch, A. Ray, The use of DTA/TGA to study the effects of ground quartz with different surface areas in autoclaved cement: quartz pastes. Use of the semi-isothermal thermogravimetric technique, Thermochimica Acta. 306 (1997) 159–165. doi:10.1016/S0040-6031(97)00279-7.
[45] W.A. Deer, R.A. Howie, J. Zussman, Rock-forming minerals : Vol. 4A, Framework silicates : Feldspars, 2. ed., The Geological Society, London, 2001.
[46] S. Mollo, M. Masotta, F. Forni, O. Bachmann, G. De Astis, G. Moore, P. Scarlato, A K-feldspar–liquid hygrometer specific to alkaline differentiated magmas, Chemical Geology. 392 (2015) 1–8. doi:10.1016/j.chemgeo.2014.11.010.
[47] Y. Wang, D. Wang, C. Dong, Y. Yang, The behaviour and reactions of sodium containing minerals in ash melting process, Journal of the Energy Institute. 90 (2017) 167–173. doi:10.1016/j.joei.2016.02.007.
[48] H. Rahier, B. Van Mele, J. Wastiels, Low-temperature synthesized aluminosilicate glasses, Journal of Materials Science. 31 (1996) 80–85. doi:10.1007/BF00355129.
[49] P. Kinnunen, H. Sreenivasan, C. Cheeseman, M. Illikainen, Phase separation in alumina-rich glasses to increase glass reactivity for low-CO2 alkali-activated cements, ((Under minor revision in Journal of Cleaner Production)).
[50] M. Knapek, T. Húlan, P. Minárik, P. Dobroň, I. Štubňa, J. Stráská, F. Chmelík, Study of microcracking in illite-based ceramics during firing, Journal of the European Ceramic Society. 36 (2016) 221–226. doi:10.1016/j.jeurceramsoc.2015.09.004.
[51] P. Pisciella, M. Pelino, Thermal expansion investigation of iron rich glass-ceramic, Journal of the European Ceramic Society. 28 (2008) 3021–3026. doi:10.1016/j.jeurceramsoc.2008.05.046.
[52] D. Kuscer, I. Bantan, M. Hrovat, B. Malič, The microstructure, coefficient of thermal expansion and flexural strength of cordierite ceramics prepared from alumina with different particle sizes, Journal of the European Ceramic Society. 37 (2017) 739–746. doi:10.1016/j.jeurceramsoc.2016.08.032.
[53] P.N. Lemougna, U.F. Chinje Melo, M.-P. Delplancke, H. Rahier, Influence of the activating solution composition on the stability and thermo-mechanical properties of inorganic polymers

(geopolymers) from volcanic ash, Construction and Building Materials. 48 (2013) 278–286. doi:10.1016/j.conbuildmat.2013.06.089.
[54] P. Duxson, G.C. Lukey, J.S.J. van Deventer, Thermal evolution of metakaolin geopolymers: Part 1 – Physical evolution, Journal of Non-Crystalline Solids. 352 (2006) 5541–5555. doi:10.1016/j.jnoncrysol.2006.09.019.
[55] M. Karhu, J. Lagerbom, S. Solismaa, M. Honkanen, A. Ismailov, M.-L. Räisänen, E. Huttunen-Saarivirta, E. Levänen, P. Kivikytö-Reponen, Mining tailings as raw materials for reaction-sintered aluminosilicate ceramics: Effect of mineralogical composition on microstructure and properties, Ceramics International. (2018). doi:10.1016/j.ceramint.2018.11.180.

FIGURE CAPTIONS

Figure 1: Effect of LDS on the green strength of referred compositions

Figure 2: Compressive strength of the synthetized specimens

Figure 3: Effect of sodium compound on the three-point flexural strength of referred compositions sintered at indicated temperatures

Figure 4: Effect of sodium compound on the water absorption and apparent density of referred compositions

Figure 5: XRD spectra of QFS and LDS

Figure 6: TG/DSC curves of QFS and LDS

Figure 7: XRD spectra of QFS and compositions nº 3, 9, 10, and 14 sintered at 900 ºC

Figure 8: Effect of sodium hydroxide in the reduction of quartz in referred compositions

Figure 9: SEM image of powdered QFS

Figure 10: SEM image of composition 3, 9 and 14 at 900 ºC

Figure 11: SEM image of compositions 3 and 9 at higher magnification and 10µm A-B line analysis in composition 9

Figure 12: Dilatometry curves of compositions nº 7, 8, 9 and 14

LIST OF TABLES

Table 1: Chemical analysis of QFS and LDS (wt%)

	SiO_2	Al_2O_3	Fe_2O_3	CaO	MgO	Na_2O	K_2O	TiO_2	P_2O_5	MnO	SUM
QFS	77.5	13.5	0.2	0.3	0.0	4.8	3.3	0.0	0.1	0.0	99.9
LDS	7.16	32.30	1.64	48.43	5.66	-	0.02	0.85	0.01	-	99.5

Table 2: Leaching test of the spodumene tailings (QFS) determined according to **SFS-EN 12457-3** and limits suggested by the Finnish regulation **(VNa 331/2013).**

	Solubility (mg/Kg)	
Hazardous elements	**QFS**	**Limits**
As	< 0,05	0.5
Ba	< 0,06	20
Cd	< 0,04	0,04
Cr	< 0,05	0,5
Cu	0,05	2
Hg	< 0,01	0,01
Mo	< 0,06	0,5
Ni	< 0,1	0,4
Pb	< 0,05	0,5
Sb	< 0,05	0,06
Se	< 0,05	0,1
Zn	< 0,6	4
DOC	26,7	500
Cl^-	< 4	800
F^-	< 2	10
SO_4^{2-}	11,6	1000

Table 3: Particle size information of QFS and LDS

Percentage of size	<10% [µm]	<25% [µm]	<50% [µm]	<75% [µm]	<80% [µm]	<90% [µm]	<95% [µm]	<99% [µm]
QFS as received	63.07	109.2	171.4	253.1	278.1	360.9	481.2	1028.1
QFS after grinding	1.765	4.016	10.70	29.15	37.62	83.15	125.6	234.5
LDS after grinding	1.295	4.525	12.34	31.45	38.00	64.93	89.18	140.3

Table 4: Mixture proportioning

Ref	QFS (g)	LDS (g)	Sodium carbonate (g)	NaOH (g)	Water (g)	Sintering temperature
1 (0wt% Na)	90	10	-	-	24	700, 800, 900ºC
2 (~1wt% Na_2CO_3)	90	10	1	-	24	
3 (~1wt% NaOH)	90	10	-	1	24	
4 (~3wt% Na_2CO_3)	90	10	3	-	24	
5 (~3wt% NaOH)	90	10	-	3	24	
6 (~5wt% Na_2CO_3)	90	10	5	-	24	
7 (~5wt% NaOH)	90	10	-	5	24	
8 (~7wt% Na_2CO_3)	90	10	7	-	24	
9 (~7wt% NaOH)	90	10	-	7	24	
10 (0wt% Na)	100	-	-	-	20	
11 (~1wt% Na_2CO_3)	100	-	1	-	22	
12 (~1wt% NaOH)	100	-	-	1	22	
13 (~3wt% Na_2CO_3)	100	-	3	-	22	
14 (~3wt% NaOH)	100	-	-	3	22	

Table 5: Elemental weight composition of points analyzed in the back scattered image of powdered QFS

Point Analysis	O	Na	Al	Si	K	Total	Ascribed mineral based on XRD analysis
1	43.34	0.58	10.39	32.03	13.66	100	Microcline ($KAlSi_3O_8$)
2	43.15	0.3	10.29	32.31	13.94	100	
3	45.95	8.69	11.16	34.2	0	100	
4	45.74	8.69	11.03	34.54	0	100	
5	46.05	8.53	11.01	34.41	0	100	Albite ($Na\,Al\,Si_3O_8$)
6	46.01	8.59	11.09	34.31	0	100	
7	46.49	6.67	10.46	32.65	3.72	100	
8	45.92	7.54	10.83	33.72	2	100	
9	50.54	0	0	49.46	0	100	Quartz (SiO_2)
10	49.87	0	0	50.13	0	100	

Table 6: Elemental weight composition of selected points from Figure 11

Point Analysis	O	Na	Al	Si	K	Ca	Fe	Mg	Mn	Ti	Total	Suggested mineral based on XRD analysis
1	50.33	0	0	49.67	0	0	0	0	0	0	100	Relic of quartz (SiO_2) particle
2	50.32	0.49	0	49.19	0	0	0	0	0	0	100	
3	44.6	7.23	5.96	34.14	3.49	1.99	2.59	0	0	0	100	Amorphous phase (melt)
4	43.6	7.42	6.15	31.94	3.23	1.95	5.71	0	0	0	100	
5	44.96	7.19	6.21	35.17	3.54	2.34	0.58	0	0	0	100	
6	45.34	6.74	9.6	33.77	3.94	0.6	0	0	0	0	100	
7	44.67	7.33	6.15	35.8	3.3	2.44	0.31	0	0	0	100	
8	45.44	7.06	5.99	35.03	3.38	2.57	0	0.52	0	0	100	
9	46.35	8.69	10.91	34.04	0	0	0	0	0	0	100	Relic of albite particles
10	46.12	8.74	10.81	34.33	0	0	0	0	0	0	100	
11	46.21	8.75	10.99	34.05	0	0	0	0	0	0	100	
12	46.11	8.69	10.91	34.29	0	0	0	0	0	0	100	
13	45.49	8.75	11.03	34.72	0	0	0	0	0	0	100	
14	49.88	0	0	50.12	0	0	0	0	0	0	100	Relic of quartz particle
15	49.03	0	0	50.97	0	0	0	0	0	0	100	
16	34.65	0	0	0	0	0	0.84	62.03	2.47	0	100	LDS particle with several crystal phases
17	37.62	0	28.38	1.9	0	30.03	0	2.07	0	0	100	
18	33.84	0	9.63	1.56	0	34.8	0	1.15	0	19.0	100	

FIGURES

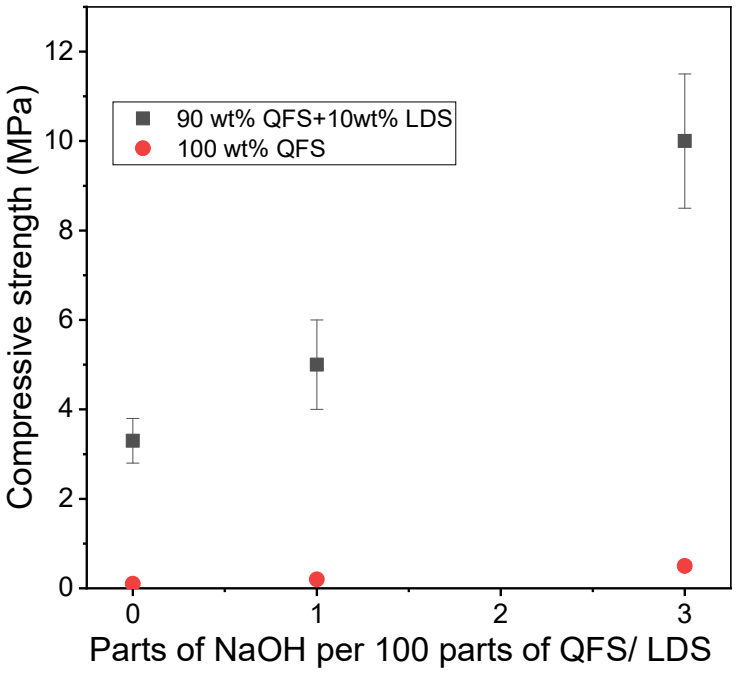

Figure 1

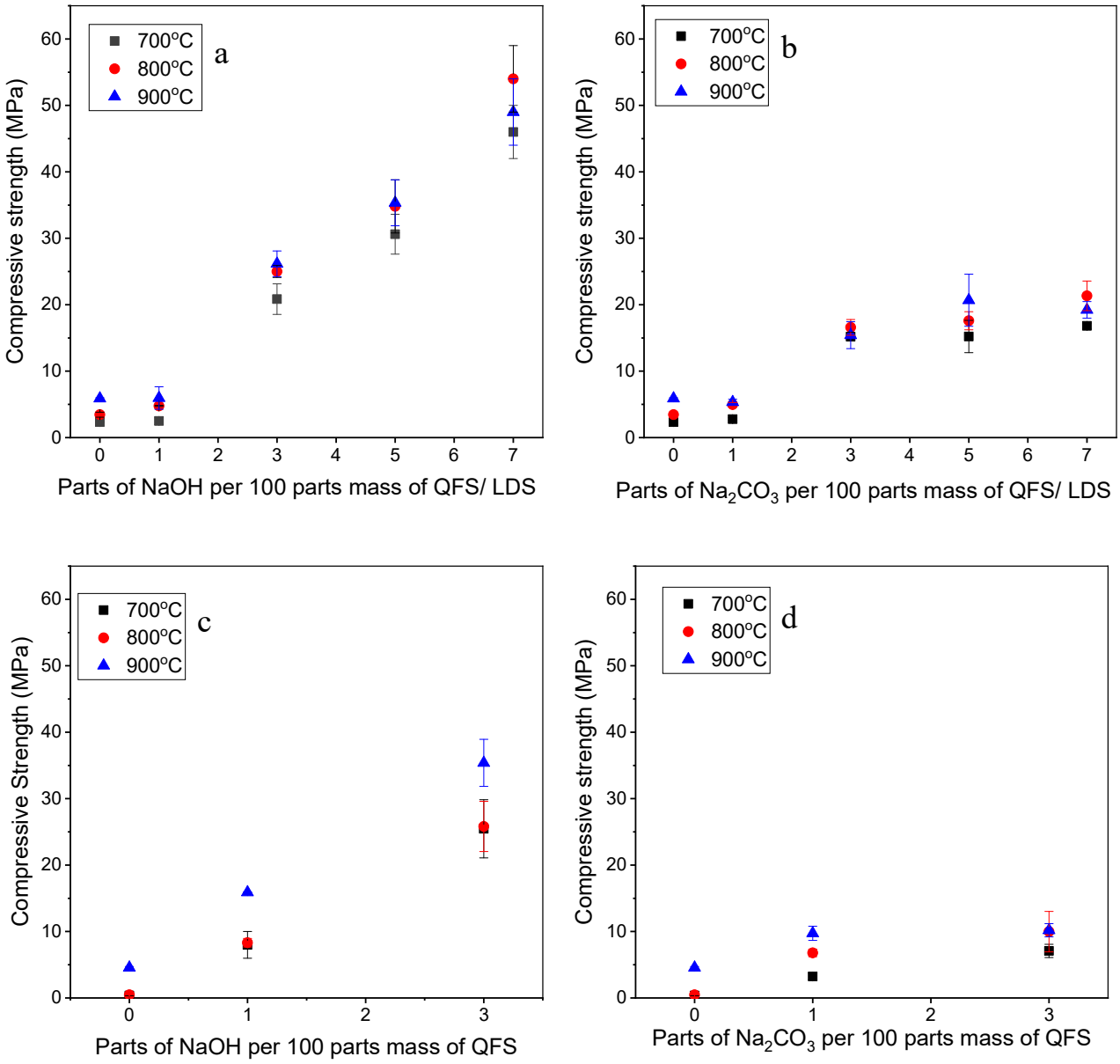
700°C
800°C
900°C
a
Compressive strength (MPa)
Parts of NaOH per 100 parts mass of QFS/ LDS
b
Parts of Na_2CO_3 per 100 parts mass of QFS/ LDS
c
Compressive Strength (MPa)
Parts of NaOH per 100 parts mass of QFS
d
Parts of Na_2CO_3 per 100 parts mass of QFS

Figure 2:

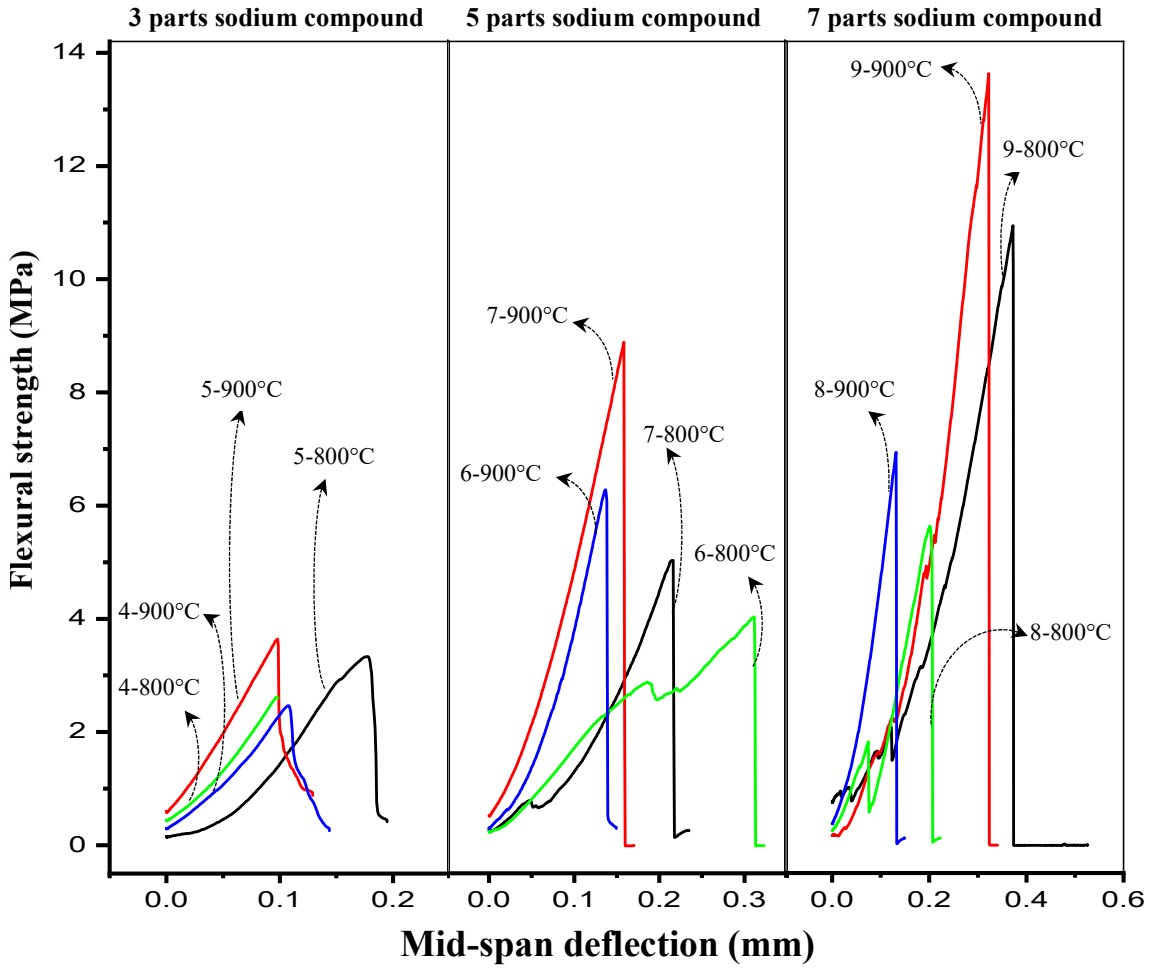
3 parts sodium compound
5 parts sodium compound
7 parts sodium compound
Flexural strength (MPa)
Mid-span deflection (mm)
4-900°C
4-800°C
5-900°C
5-800°C
6-900°C
7-900°C
7-800°C
6-800°C
8-900°C
9-900°C
9-800°C
8-800°C

Figure 3:

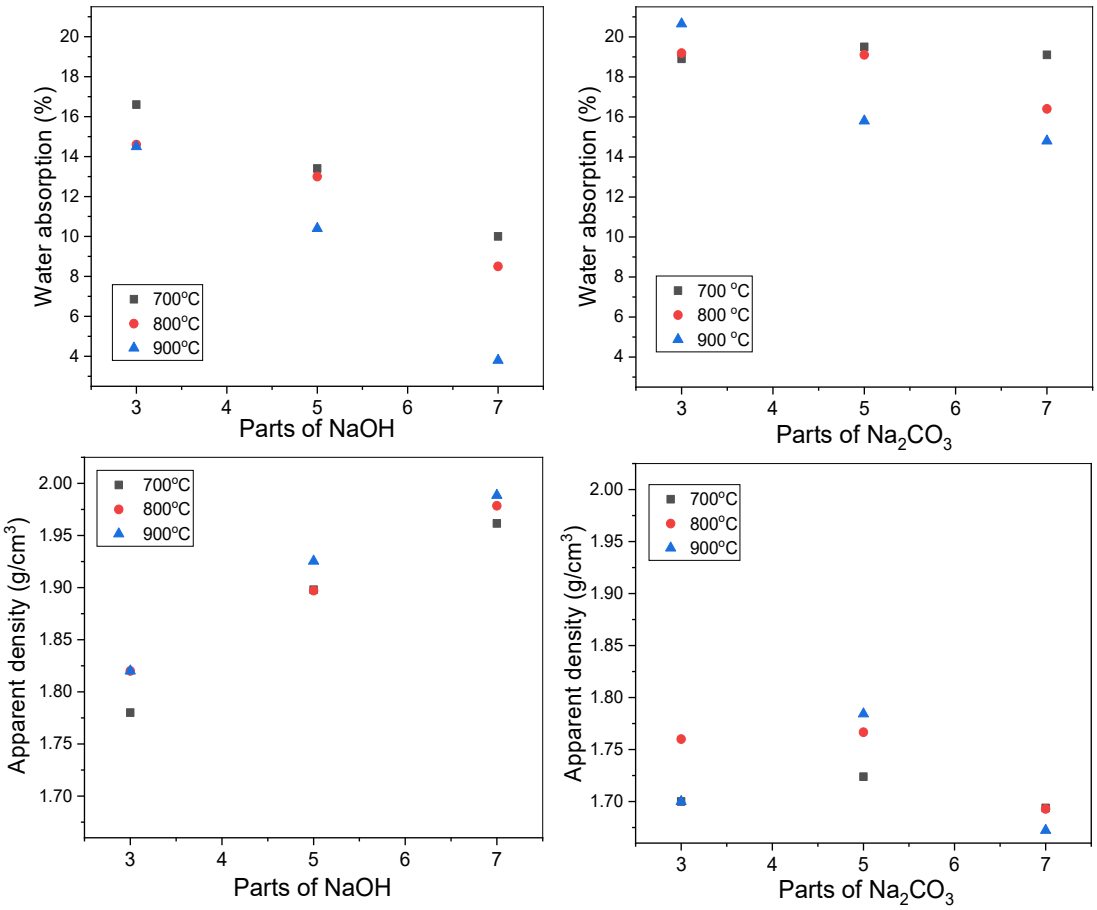
Water absorption (%)
Parts of NaOH
700°C
800°C
900°C
Water absorption (%)
Parts of Na_2CO_3
700 °C
800 °C
900 °C
Apparent density (g/cm^3)
Parts of NaOH
700°C
800°C
900°C
Apparent density (g/cm^3)
Parts of Na_2CO_3
700°C
800°C
900°C

Figure 4:

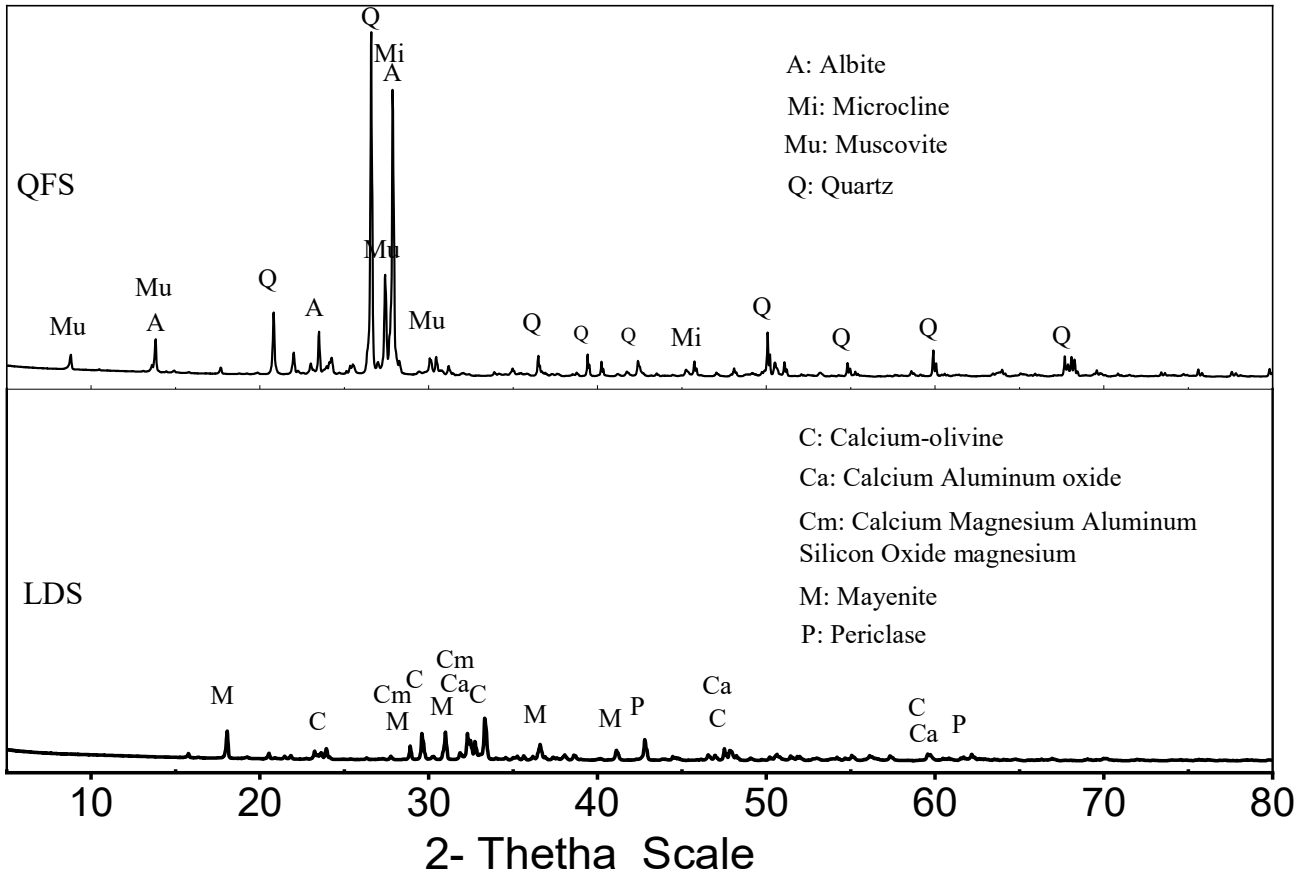
QFS
A: Albite
Mi: Microcline
Mu: Muscovite
Q: Quartz
LDS
C: Calcium-olivine
Ca: Calcium Aluminum oxide
Cm: Calcium Magnesium Aluminum Silicon Oxide magnesium
M: Mayenite
P: Periclase
10
20
30
40
50
60
70
80
2- Thetha Scale

Figure 5:

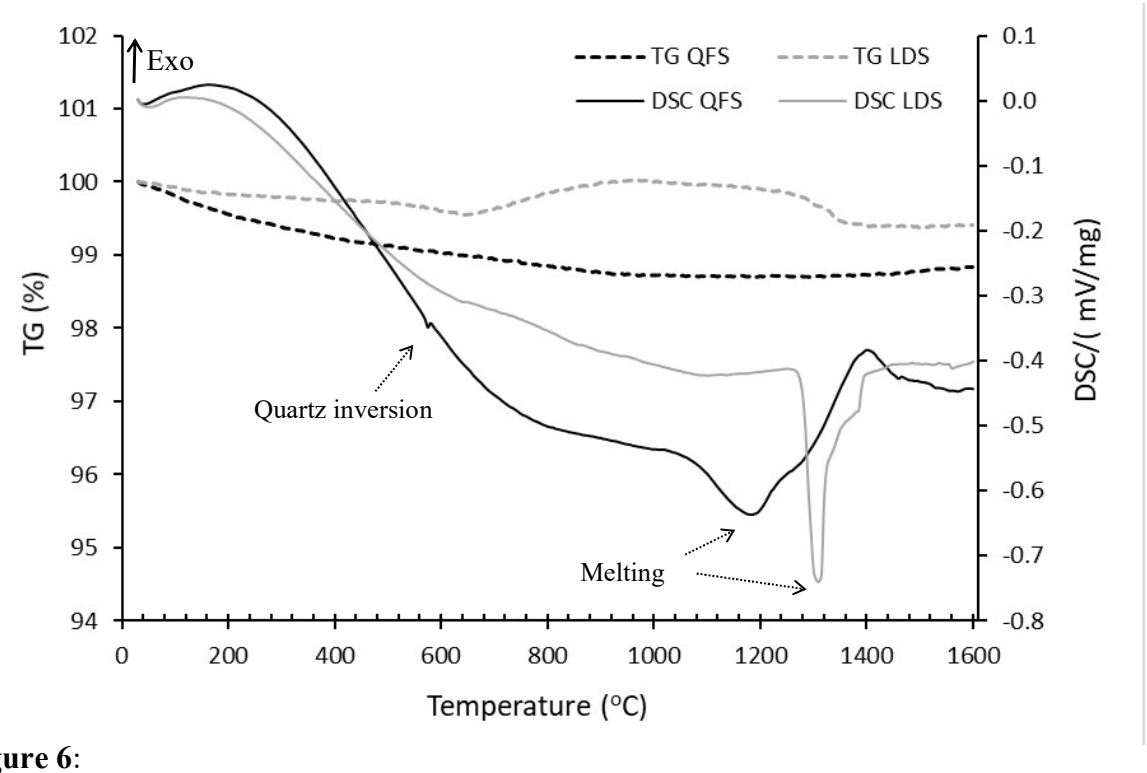
Exo
TG QFS
TG LDS
DSC QFS
DSC LDS
Quartz inversion
Melting
TG (%)
DSC/(mV/mg)
Temperature (°C)
102
101
100
99
98
97
96
95
94
0.1
0.0
-0.1
-0.2
-0.3
-0.4
-0.5
-0.6
-0.7
-0.8
0
200
400
600
800
1000
1200
1400
1600

Figure 6:

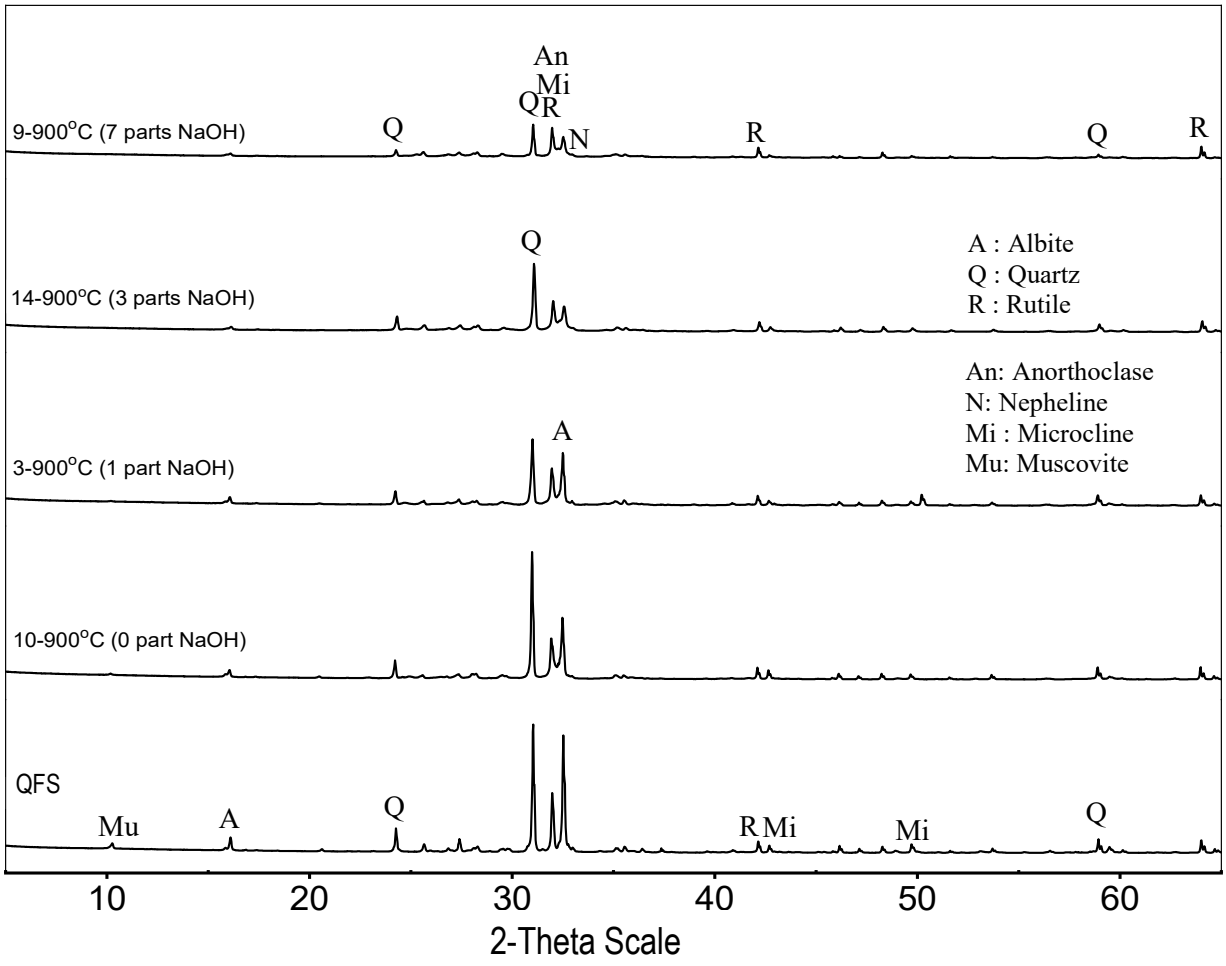
An
Mi
Q
R
9-900°C (7 parts NaOH)
Q
N
R
Q
R
14-900°C (3 parts NaOH)
Q
A : Albite
Q : Quartz
R : Rutile
An: Anorthoclase
N: Nepheline
Mi : Microcline
Mu: Muscovite
3-900°C (1 part NaOH)
A
10-900°C (0 part NaOH)
QFS
Mu
A
Q
R Mi
Mi
Q
10
20
30
40
50
60
2-Theta Scale

Figure 7:

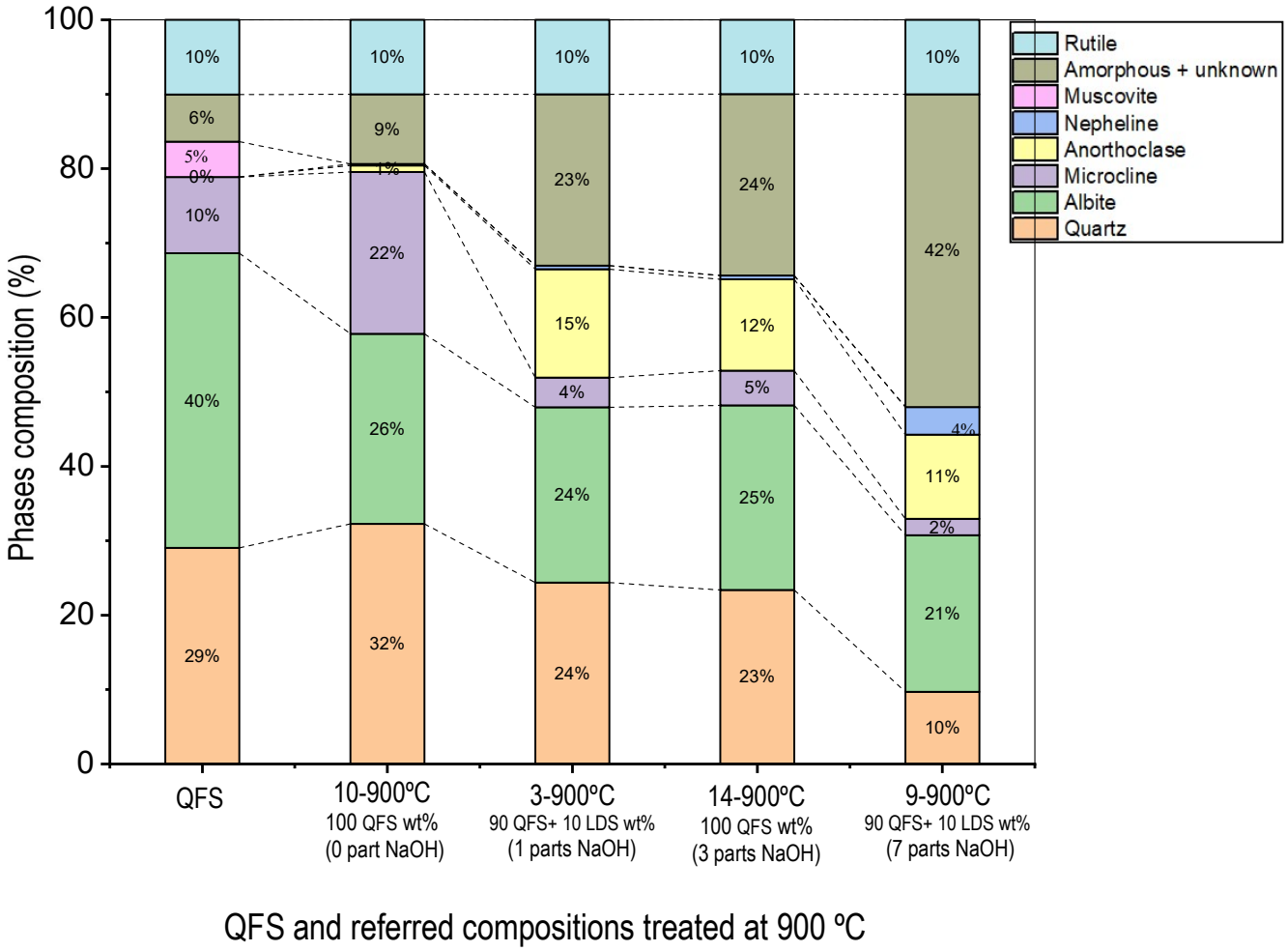
Phases composition (%)
100
80
60
40
20
0
Rutile
Amorphous + unknown
Muscovite
Nepheline
Anorthoclase
Microcline
Albite
Quartz
10%
6%
5%
6%
10%
40%
29%
10%
9%
1%
22%
26%
32%
10%
23%
15%
4%
24%
24%
10%
24%
12%
5%
25%
23%
10%
42%
4%
11%
2%
21%
10%
QFS
10-900ºC
100 QFS wt%
(0 part NaOH)
3-900ºC
90 QFS+ 10 LDS wt%
(1 parts NaOH)
14-900ºC
100 QFS wt%
(3 parts NaOH)
9-900ºC
90 QFS+ 10 LDS wt%
(7 parts NaOH)
QFS and referred compositions treated at 900 ºC

Figure 8:

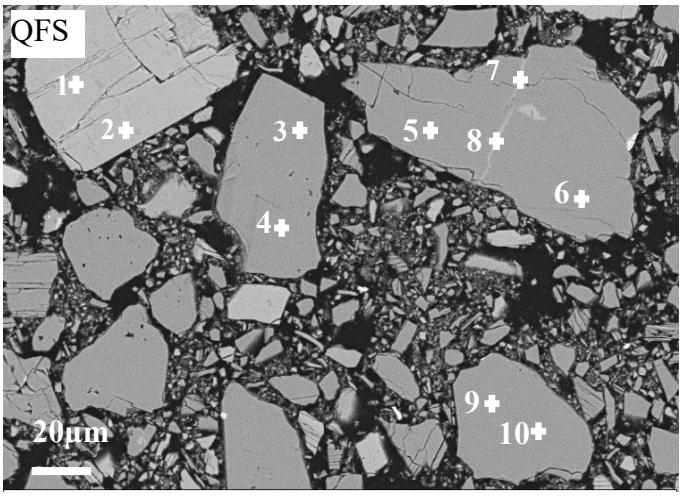

Figure 9:

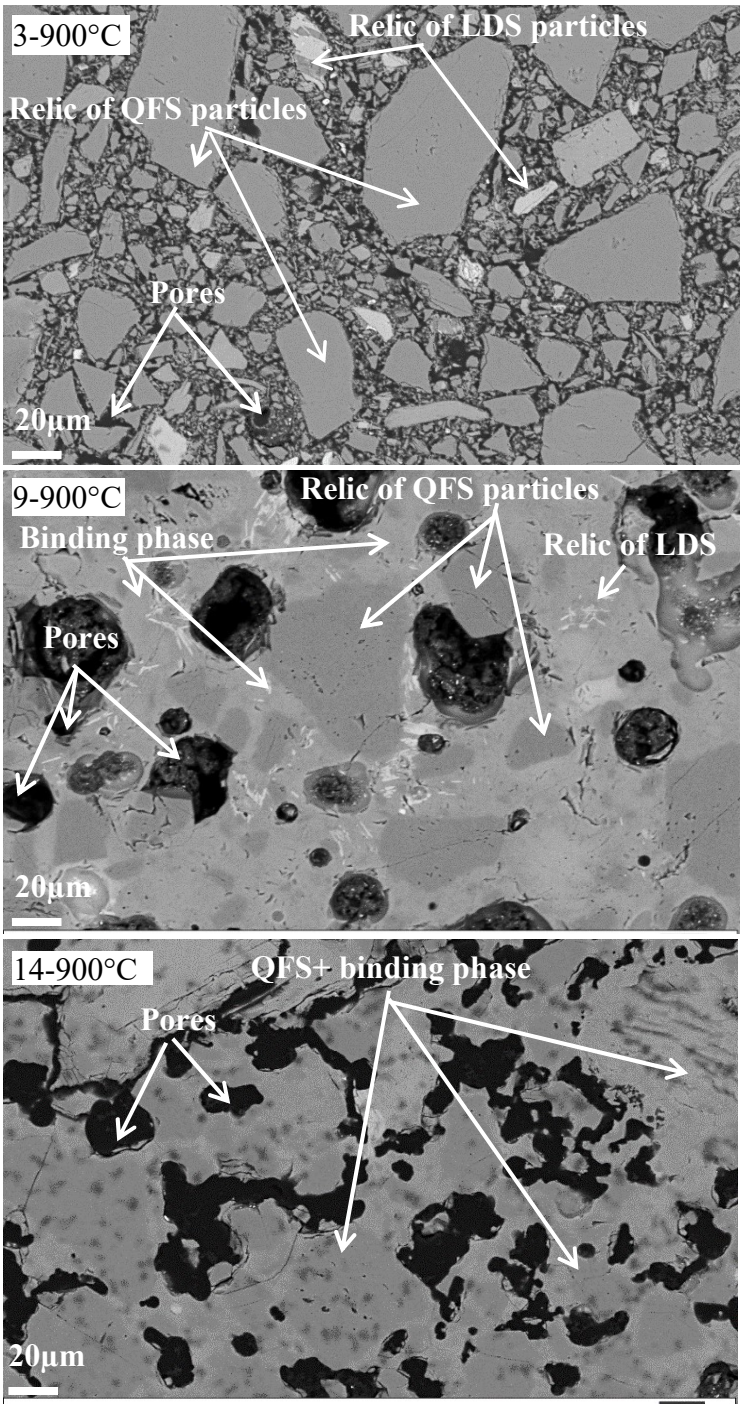
3-900°C
Relic of LDS particles
Relic of QFS particles
Pores
20µm
9-900°C
Relic of QFS particles
Binding phase
Relic of LDS
Pores
20µm
14-900°C
QFS+ binding phase
Pores
20µm

Figure 10:

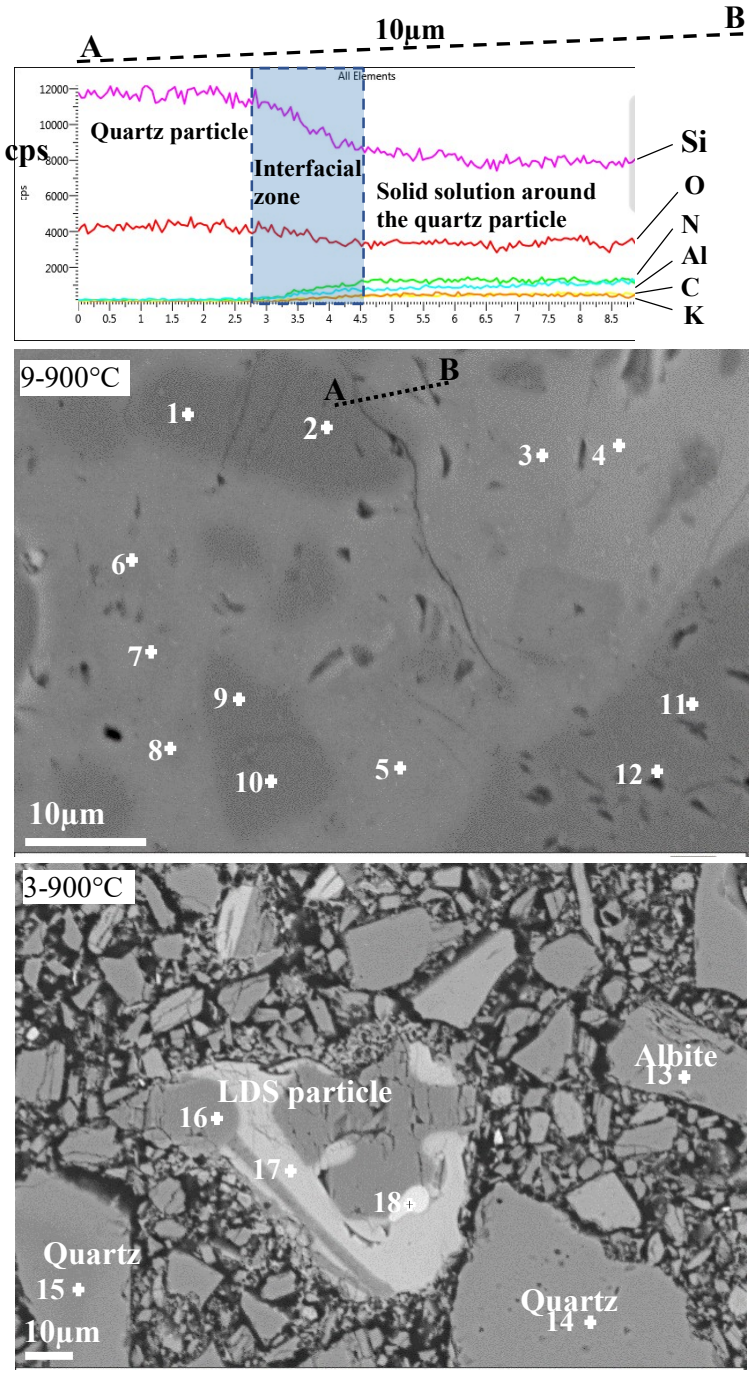
A
10µm
B
All Elements
cps
Quartz particle
Interfacial zone
Solid solution around the quartz particle
Si
O
N
Al
C
K
9-900°C
A
B
1
2
3
4
5
6
7
8
9
10
11
12
10µm
3-900°C
Albite
13
LDS particle
16
17
18
Quartz
15
Quartz
14
10µm

Figure 11:

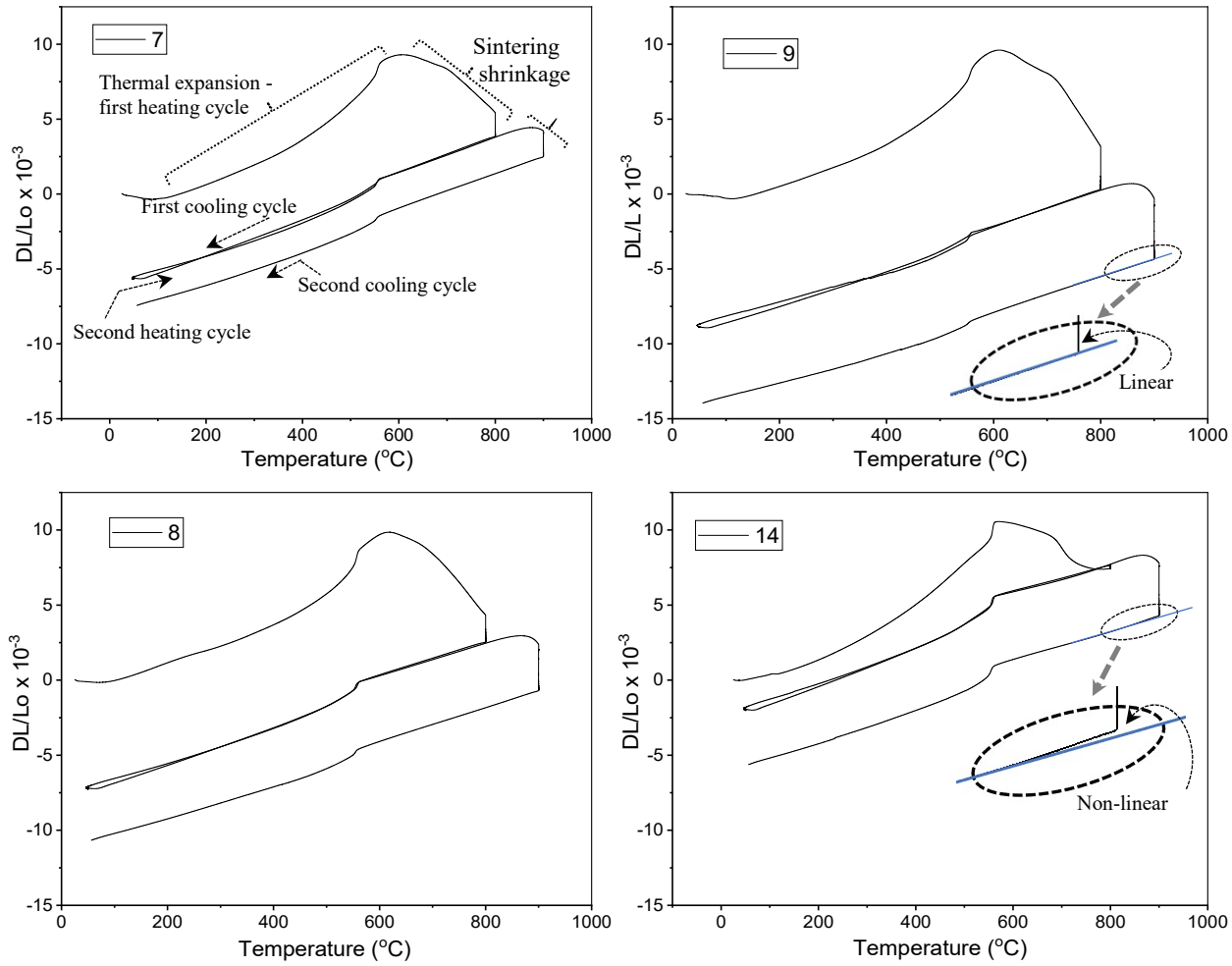
7
Thermal expansion -
first heating cycle
Sintering
shrinkage
First cooling cycle
Second cooling cycle
Second heating cycle
DL/Lo x 10-3
Temperature (°C)
9
Linear
DL/L x 10-3
Temperature (°C)
8
DL/Lo x 10-3
Temperature (°C)
14
Non-linear
DL/Lo x 10-3
Temperature (°C)

Figure 12: